

# Upper and Lower Flammability Limits, Limit N<sub>2</sub>O Concentrations, and Minimum Inerting Concentrations of n-Alkane–N<sub>2</sub>O–Diluent Mixtures: An Experimental and Computational Study

Yusuke Koshiba <sup>a, \*</sup>, Shiho Asano <sup>b</sup>

<sup>a</sup> Department of Materials Science and Chemical Engineering, Faculty of Engineering, Yokohama National University, 79-5 Tokiwadai, Hodogaya-ku, Yokohama 240-8501, Japan

<sup>b</sup> Graduate School of Environmental and Information Sciences, Yokohama National University, 79-7 Tokiwadai, Hodogaya-ku, Yokohama 240-8501, Japan

## KEYWORDS

Nitrous oxide; Lower and upper flammability limits; Limit N<sub>2</sub>O concentration; Minimum inerting concentration; Alkane; UFL estimation

## ABSTRACT

**Objectives:** N<sub>2</sub>O is widely used in the chemical industry and laboratories; however, several fire/explosion accidents have been reported in facilities that handle N<sub>2</sub>O. This study aimed (i) to experimentally investigate the lower and upper flammability limits (LFL and UFL, respectively),

limit nitrous oxide concentration (LN<sub>2</sub>OC), and minimum inerting concentrations (MICs) of fuel–N<sub>2</sub>O–diluent mixtures and (ii) to computationally estimate the UFLs of fuel–N<sub>2</sub>O–diluent mixtures.

**Methods:** Herein, methane and n-propane and nitrogen (N<sub>2</sub>), argon (Ar), and carbon dioxide (CO<sub>2</sub>) were used as fuels and diluents, respectively. The LFL, UFL, LN<sub>2</sub>OC, and MICs of the fuel–N<sub>2</sub>O–diluent mixtures were experimentally determined using a closed cylindrical vessel, and their UFLs were computationally estimated based on the laws of conservation energy and mass and adiabatic flame temperatures.

**Results:** Flammability-limit experiments revealed the following: (i) the LFLs of the CH<sub>4</sub>–N<sub>2</sub>O–diluent and C<sub>3</sub>H<sub>8</sub>–N<sub>2</sub>O–diluent mixtures were 2.5 and 1.4 vol%, respectively, (ii) the UFLs of the CH<sub>4</sub>–N<sub>2</sub>O–diluent and C<sub>3</sub>H<sub>8</sub>–N<sub>2</sub>O–diluent mixtures were 40.5 and 24.0 vol%, respectively, (iii) a nearly linear relationship between the UFL and diluent concentration was found, and (iv) the order of MICs in N<sub>2</sub>O atmosphere was consistent with the inerting ability of the diluents. Calculations based on overall combustion reactions and the laws of energy and mass conservation using six and five chemicals successfully estimated the UFLs of the CH<sub>4</sub>–N<sub>2</sub>O–diluent and C<sub>3</sub>H<sub>8</sub>–N<sub>2</sub>O–diluent mixtures with mean absolute percentage errors of  $\leq 2.8\%$  and  $\leq 4.1\%$ , respectively.

**Conclusions:** The semi-empirical model suggested herein allows accurate estimation of the UFLs of the tested fuel–N<sub>2</sub>O–diluent mixtures. These findings would contribute to reducing accident-induced losses in the chemical industry and laboratories handling N<sub>2</sub>O.

## 1. INTRODUCTION

### 1.1 Backgrounds

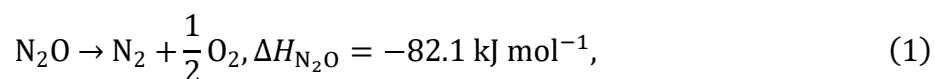
Various flammable gases posing substantial fire and explosion hazards are used as reactants and fuels in the chemical industry and laboratories. A fire and explosion accident at a chemical plant can result in loss of life/property and environmental damage. Even minor fires and explosions in the chemical industry may be widely publicized and cause public concern, eroding people's trust, as technological accidents are perceived as potentially sensational.<sup>1</sup> Thus, understanding explosion characteristics (e.g., lower/upper flammability limits) is critical for assessing fire/explosion risks and achieving safe operations.

In the chemical industry, oxygen (O<sub>2</sub>) gas is an ideal oxidizer that generally generates no byproducts during oxidation processes. Thus, O<sub>2</sub> gas is frequently used in chemical processes such as acetaldehyde production (known as the Wacker process)<sup>2</sup> and acrylonitrile production (ammoxidation, also known as the SOHIO process)<sup>3</sup>.

Similar to O<sub>2</sub>, nitrous oxide (N<sub>2</sub>O; CAS RN: 10024-97-2) is used as an oxidizer in chemical processes. The advantages of using N<sub>2</sub>O lie in the fact that (i) N<sub>2</sub>O containing ca. 36% active oxygen by mass in the molecule is an inexpensive and atom-economic oxidant<sup>4</sup>, (ii) N<sub>2</sub>O is a thermochemically stable compound under ambient conditions, (iii) N<sub>2</sub>O can be stored as a compressed liquid, which means that the storage volume can be reduced, and (iv) byproducts from N<sub>2</sub>O during oxidation reactions are environmentally friendly N<sub>2</sub> and O<sub>2</sub>. Thus, despite its high ozone-depletion and global warming potential, the unique oxidizer N<sub>2</sub>O is being studied.<sup>5, 6</sup> For instance, Parfenov et al.<sup>7</sup> delivered a new gas-phase selective oxidation of n-butenes—raw materials for methyl ethyl ketone—in the presence of N<sub>2</sub>O. Vaillant et al.<sup>8</sup> discovered a novel catalytic synthesis method for phenols, which are essential raw materials in the chemical industry, using N<sub>2</sub>O. Cornell et al.<sup>9</sup> reported a kinetic study of ammonia oxidation using N<sub>2</sub>O in a jet-stirred

reactor, as ammonia is exclusively oxidized under conditions, where N<sub>2</sub>O-rich O<sub>2</sub> oxidizers are present.

However, explosion accidents in industrial facilities handling/storing N<sub>2</sub>O have been reported. In 2016, a N<sub>2</sub>O trailer explosion in Florida, the United States, killed one employee<sup>10</sup>, whereas, in 2001, a N<sub>2</sub>O explosion in Eindhoven, the Netherlands, injured 10 people.<sup>11</sup> This reflects the fact that N<sub>2</sub>O is prone to decompose to N<sub>2</sub> and O<sub>2</sub> under elevated pressure and temperature conditions (Eq. (1)).



where  $\Delta H_{\text{N}_2\text{O}}$  denotes the enthalpy of formation.

## 1.2 Literature review

A fuel (gas/vapor)–oxidizer mixture will only burn if the fuel concentration lies within limits. When the fuel concentration of the mixture is lower than the lower flammability limit (LFL), flame propagation will not be observed owing to fuel lean conditions for combustion. In a situation, where it is higher than the upper flammability limit (UFL), the mixture will not also burn due to fuel rich conditions.<sup>12</sup> In short, a mixture is flammable when the fuel concentration is between these limits. LFL and UFL are typically interchangeable with the lower and upper explosion limits, respectively.<sup>13</sup>

Despite the unique and effective oxidizing properties described in [Section 1.1](#), few data on the flammability limits of hydrocarbon–N<sub>2</sub>O mixtures have been hitherto available in the literature.<sup>14–</sup>

<sup>17</sup> Inerting flammable mixtures with diluents is a useful approach to reduce explosion and fire risks

<sup>13, 18</sup>; however, the flammability limits of hydrocarbon–N<sub>2</sub>O mixtures diluted with inert gases such as N<sub>2</sub>, Ar, and carbon dioxide (CO<sub>2</sub>) are extremely limited in the literature.

Among the explosion characteristics of a flammable mixture, this study focuses on UFL, as well as LFL, limit nitrous oxide concentration (LN<sub>2</sub>OC), and minimum inerting concentration (MIC). LN<sub>2</sub>OC is the concentration below which any mixture does not support flame propagation, which corresponds to the limit oxygen concentration for mixtures in which the oxidizer is O<sub>2</sub>.<sup>19</sup> MIC, which is also known as the critical inerting concentration, peak concentration, diluent limit, and inert point, is the lowest inert concentration above which a mixture is non-flammable.

Generally, accurately predicting UFLs is difficult. To date, many scholars have challenged this issue to be solved. Jones<sup>20</sup> of the U.S. Bureau of Mines reported the empirical equation for UFLs (Eq. (2)) using UFL data on (normal chain/cyclic) hydrocarbons, olefins, acetylene, aromatics, turpentine, alcohols, aldehydes, ethers, ketones, acids, esters, H<sub>2</sub>, CO, nitrogen compounds, oxides, sulfides, chlorides, and bromides:

$$UFL = k C_{st} \quad (2)$$

where  $k$  represents the constant (i.e., 3.5) and  $C_{st}$  denotes the stoichiometric concentration of fuel. Note that the standard deviation of  $k$  is 2.2, implying the low prediction accuracy of the equation. Kondo et al., who proposed a semi-empirical extended Le Chatelier's equation of methane (CH<sub>4</sub>), propane (C<sub>3</sub>H<sub>8</sub>), propylene, methyl formate, and 1,1-difluoroethane, reported an overall mean absolute percentage error (MAPE (Eq. (3)) of 1.1% for their UFLs.<sup>21</sup> Lazzús, who used a 328-compound dataset, estimated UFL values with an MAPE <7.1% using a neural network based on particle swarm optimization.<sup>22</sup>

$$\text{MAPE} = \frac{100}{n} \sum_{k=1}^n \left| \frac{V_{e,k} - V_{a,k}}{V_{a,k}} \right|, \quad (3)$$

where  $V_e$  and  $V_a (\neq 0)$  denote the estimated and actual values, respectively, and  $n$  represents the number of data points. A low MAPE indicates high accuracy in the model. Kondo et al., who used a 99-compound dataset, demonstrated an MAPE value of 14.6% for UFLs by proposing an empirical  $F$ -number ( $F = 1 - (\text{LFL}/\text{UFL})^{0.5}$ ).<sup>23</sup> A number of researchers have estimated UFLs using a structural group contribution method, which divides a molecule into groups (e.g., functional groups); for instance, Albahri<sup>24</sup> used a 464-compound dataset and provided an MAPE of 11.8%. However, the primary weakness of the group contribution method is that the model accuracy is strongly influenced by the dataset used.<sup>25</sup> More importantly, the model cannot estimate the UFL of a molecule with functional groups not included in the dataset or distinguish isomers.<sup>26</sup>

Thus far, related scholars have reported the estimation methods of UFLs focusing on adiabatic flame temperatures (AFTs). Liaw et al.<sup>27</sup> in their investigation of the UFLs of fuel–air–diluent mixtures (diluent:  $\text{N}_2$  and  $\text{CO}_2$ ) using fixed AFTs observed that the accurate estimation of the UFLs of mixtures is generally challenging because of incomplete combustion at UFLs. Mitu et al. demonstrated a method to estimate the flammability limits of ester–air–diluent mixtures using extended AFT profiles.<sup>28</sup> Wu et al., who studied the ULFs of alkane (i.e., propane, n-butane, and isopentane)–air– $\text{CO}_2$  mixtures, reported a good estimation approach using a variable AFT method and demonstrated an MAPE of  $<3.5\%$ .<sup>29</sup> Koshiba et al.<sup>30</sup> reported an MAPE of  $\leq 1.0\%$  for binary hydrocarbons (i.e., methane, ethane, ethylene, and propylene)– $\text{N}_2\text{O}$  mixtures using the variable AFT method.

### 1.3 Objectives of this study

In this study, the UFLs, LFLs, LN<sub>2</sub>OC, and MICs of straight-chain hydrocarbon (CH<sub>4</sub> and C<sub>3</sub>H<sub>8</sub>)–N<sub>2</sub>O–diluent (N<sub>2</sub>, Ar, and CO<sub>2</sub>) mixtures were experimentally investigated. Thus, the number of combinations was six: CH<sub>4</sub>–N<sub>2</sub>O–N<sub>2</sub>, CH<sub>4</sub>–N<sub>2</sub>O–Ar, CH<sub>4</sub>–N<sub>2</sub>O–CO<sub>2</sub>, C<sub>3</sub>H<sub>8</sub>–N<sub>2</sub>O–N<sub>2</sub>, C<sub>3</sub>H<sub>8</sub>–N<sub>2</sub>O–Ar, and C<sub>3</sub>H<sub>8</sub>–N<sub>2</sub>O–CO<sub>2</sub>. Furthermore, the UFLs of these mixtures, which are generally difficult to predict, were computationally estimated on the basis of overall combustion reactions and the laws of conservation of energy and mass.

The rest of this paper is structured as follows: [Section 2](#) explains the experimental and calculation methods of UFLs. [Section 3](#) presents and discusses the experimental and calculation results. [Section 4](#) provides the study conclusions.

## 2. METHODOLOGY

### 2.1. Experimental methods

#### 2.1.1. Chemicals

CH<sub>4</sub> (purity: >99.999%; CAS RN: 74-82-8), C<sub>3</sub>H<sub>8</sub> (purity: >99.99%; CAS RN:74-98-6), N<sub>2</sub>O (purity: >99.99%), N<sub>2</sub> (purity: >99.99%), Ar (purity: >99.995%), and CO<sub>2</sub> (purity: >99.99%). All gases were purchased from a gas supplier (Suzuki Shokan Co., Ltd., Japan) and were thoroughly dried (H<sub>2</sub>O: <15 ppm).

#### 2.1.2. Experimental procedures

Flammability limits were determined using the experimental apparatus shown in Figure 1, which is the same as that used for an earlier study.<sup>31</sup> The closed cylindrical stainless-steel vessel with an internal height of 120 mm and an internal diameter of 100 mm (i.e., ca. 0.94 dm<sup>3</sup>) has a stainless-steel stirrer with a mixing rate of 1000 rpm, pointed tungsten electrodes with a diameter of 1.0 mm, and two pressure transducers. The Swagelok PTI-S pressure transducer (USA) located on the top of the vessel and the Kyowa PGM-H pressure transducer (Japan) placed on the vessel wall were used to monitor the partial pressures of component gases and explosion pressures, respectively. The PGM-H pressure transducer and ignition electrodes were located at the same height. Explosion pressure histories were recorded on a personal computer using the NR-500 and NR-ST04 measuring units (Keyence Co., Japan).

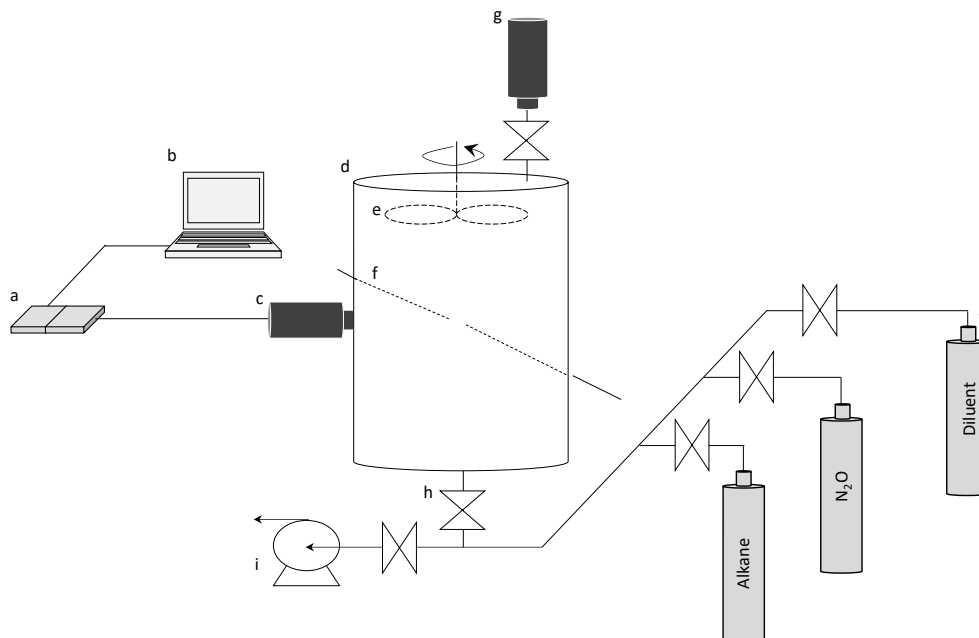


Figure 1 Schematic of experimental apparatus for flammability limit tests. (a) Strain measuring units, (b) personal computer, (c) pressure transducer for measuring explosion pressure, (d) explosion vessel, (e) stirrer, (f) electrode for ignition, (g) pressure transducer for preparing gas mixtures, (h) valve, (i) vacuum pump, and (j) gas cylinder.

Before performing the flammability-limit tests, the vessel was sufficiently evacuated using a vacuum pump to a pressure of approximately  $6.7 \times 10^{-1}$  Pa. The gas mixtures were prepared using the partial pressure method and then mechanically mixed using the stirrer at a speed of 1,000 rpm for at least 1 min. We confirmed that stirring the mixtures for either 1 or 3 min had no considerable effect on the flammability limits of the tested mixtures. Under the quiescent conditions, an electric spark with an energy of 18 J ( $9.00 \times 10^3$  V,  $2.0 \times 10^{-2}$  A, and  $1.0 \times 10^{-1}$  s), which was powered with a neon transformer, was discharged between the electrodes to ignite each gas mixture at the center of the vessel.

Each test was conducted at an initial temperature of approximately 25 °C and initial pressure of 101.3 kPa and repeated thrice to verify the reproducibility of the experimental results. Data through the strain measuring units were collected using the electric discharges as triggers. In this study, a 5% pressure-rise criterion was applied.<sup>32</sup>

## **2.2. Calculation methods**

### **2.2.1. Thermochemical equilibrium calculations**

Thermochemical equilibrium calculations were performed to compute the upper-limit mixture's equilibrium compositions and AFTs, which are theoretical temperatures under the

assumption of an adiabatic condition, using a chemical kinetics simulator based on the Gibbs free energy minimization method, CHEMKIN (ver. 4.1.1).<sup>33</sup> For the tested n-alkane–N<sub>2</sub>O–diluent mixtures, the thermochemical equilibrium calculations used the following 35 chemical species: CO, CO<sub>2</sub>, CH, CH<sub>2</sub>, CH<sub>3</sub>, CH<sub>4</sub>, HCO, CN, C, C<sub>2</sub>H<sub>2</sub>, C<sub>2</sub>H<sub>4</sub>, C<sub>2</sub>H<sub>5</sub>, C<sub>2</sub>H<sub>6</sub>, C<sub>2</sub>, C<sub>3</sub>, C<sub>3</sub>H<sub>8</sub>, C<sub>4</sub>, C<sub>5</sub>, C<sub>6</sub>H<sub>6</sub>, OH, H, H<sub>2</sub>, HO<sub>2</sub>, H<sub>2</sub>O, H<sub>2</sub>O<sub>2</sub>, O, O<sub>2</sub>, N, NO, NO<sub>2</sub>, N<sub>2</sub>, N<sub>2</sub>O, NH, HNO, and Ar.<sup>12</sup>

In the thermochemical equilibrium calculations, the thermodynamic coefficients,  $a_1$ – $a_7$ , of the alkanes in Eqs. (4)–(6) extracted from a thermodynamic database<sup>34</sup> were used.

$$\frac{c_p}{R} = \sum_{k=1}^5 a_k T^{k-1}, \quad (4)$$

$$\frac{H}{RT} = \left( \sum_{k=1}^5 \frac{a_k}{k} T^{k-1} \right) + \frac{a_6}{T}, \quad (5)$$

$$\frac{S}{R} = a_1 \cdot \ln T + \left( \sum_{k=2}^5 \frac{a_k}{k-1} T^{k-1} \right) + \frac{a_7}{T}, \quad (6)$$

where  $c_p$ ,  $R$ ,  $T$ ,  $H$ , and  $S$  represent the heat capacity, gas constant, temperature, enthalpy, and entropy, respectively. In the calculations, each component chemical species was postulated to act as an ideal gas (Eq. (7)):

$$P = \sum X_k RT, \quad (7)$$

where  $P$  and  $X_k$  denote the pressure and molar concentration of chemical species  $k$ , respectively.

### 2.2.2. Estimation methods of UFLs

In this study, according to related researchers<sup>29, 35</sup>, the UFLs of the n-alkane–N<sub>2</sub>O–diluent mixtures were estimated under the following assumption: (I) combustion reactions at UFLs proceed at constant pressure, (II) AFT values vary with the diluent concentration, and (III) the fuels are oxidized to yield carbon monoxide (CO) and hydrogen (H<sub>2</sub>), and subsequently, H<sub>2</sub>O and CO<sub>2</sub> are produced via H<sub>2</sub> and CO oxidation processes, respectively. Assumption (II) is reasonable, as Mitu et al.<sup>36</sup> also reported the dependency of the AFT on the diluent concentration. Assumption (III) reflects the facts that (i) the consumption of a fuel molecule and its decomposition fragments (e.g., CH<sub>3</sub> radical) is strongly driven by reactions with radicals (e.g., O and H) in combustion reactions<sup>37</sup> and (ii) the pathway of the reaction of CO with hydroxyl radical (CO + •OH → CO<sub>2</sub> + •H) is the primary source of CO<sub>2</sub> production; CO is mostly left in cases, where the concentration of •OH radical is insufficient to initiate the CO + •OH reaction. In brief, CO<sub>2</sub> is produced in stepwise oxidation reactions. CO is primarily produced because of incomplete combustion for upper-limit mixtures.

Based on the above findings of the earlier studies, the major chemical species of the upper-limit mixtures were CO, CO<sub>2</sub>, H<sub>2</sub>O, H<sub>2</sub>, and diluent (i.e., N<sub>2</sub>).<sup>38</sup> For the n-alkane–N<sub>2</sub>O–diluent mixtures tested in this study, except for the n-alkane–N<sub>2</sub>O–Ar mixture, the following five chemical species were selected in the calculations: CO, CO<sub>2</sub>, H<sub>2</sub>O, H<sub>2</sub>, and N<sub>2</sub>. For the n-alkane–N<sub>2</sub>O–Ar mixture, the six chemical species—CO, CO<sub>2</sub>, H<sub>2</sub>O, H<sub>2</sub>, N<sub>2</sub>, and Ar—were used; in short, Ar was added.

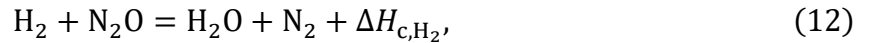
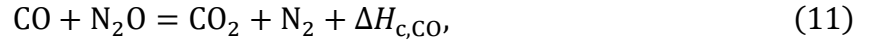
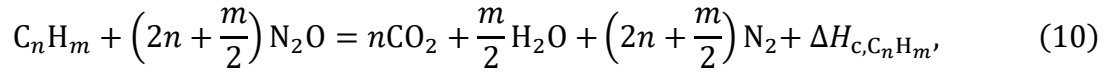
For the upper-limit n-alkane–N<sub>2</sub>O–diluent mixtures, the overall reaction was assumed (Eqs. (8) and (9)).

$$U_k C_n H_m + (1 - U_k - y) N_2 O + y D = \alpha_1 CO + \alpha_2 CO_2 + \alpha_3 H_2 O + \alpha_4 H_2 + \alpha_5 N_2 + z D + \Delta H_c, \quad (8)$$

with

$$m = 2n + 2, \quad (9)$$

where  $U_k$  denotes the UFL of alkane,  $n$  and  $m$  represent the numbers of carbon and hydrogen in the n-alkane, respectively,  $y$  represents the molar fraction of diluent in the mixtures,  $\alpha_1$ – $\alpha_5$  and  $z$  denote the stoichiometric coefficients in the overall reaction, and  $\Delta H_c$  denotes the enthalpy of the combustion reaction. The complete combustion reactions for each component species in Eq. (8) are presented in Eqs. (10)–(12).



where  $\Delta H_{c, C_n H_m}$ ,  $\Delta H_{c, CO}$ , and  $\Delta H_{c, H_2}$  represent the enthalpy of the combustion reactions for  $C_n H_m$ , CO, and  $H_2$ , respectively.

Substituting Eqs. (10)–(12) into Eq. (8) yields the following equation (Eq. (13)).

$$\Delta H_c = U_k \cdot \Delta H_{c, C_n H_m} - \alpha_1 \cdot \Delta H_{c, CO} - \alpha_4 \cdot \Delta H_{c, H_2} \quad (13)$$

Taking the law of energy conservation into consideration, the following equation is obtained (Eq. (14)):

$$\begin{aligned} \alpha_1 H_{CO}^0 + \alpha_2 H_{CO_2}^0 + \alpha_3 H_{H_2O}^0 + \alpha_4 H_{H_2}^0 + \alpha_5 H_{N_2}^0 + y H_D^0 + \Delta H_c \\ = \alpha_1 H_{CO}^{ad} + \alpha_2 H_{CO_2}^{ad} + \alpha_3 H_{H_2O}^{ad} + \alpha_4 H_{H_2}^{ad} + \alpha_5 H_{N_2}^{ad} + z H_D^{ad} \end{aligned} \quad (14)$$

where  $H_k^0$  and  $H_k^{ad}$  denote the enthalpy of chemical species  $k$  at 25 °C and the AFT, respectively. As mentioned previously,  $H$  values were calculated using Eq. (5). Based on the law of mass conservation, we can obtain the following Eqs. (15)–(19) for C, H, O, N, and Ar elements.

$$nU_k = \alpha_1 + \alpha_2 \quad (15)$$

$$mU_k = 2(\alpha_3 + \alpha_4) \quad (16)$$

$$1 - U_k - y = \alpha_1 + 2\alpha_2 + \alpha_3 \quad (17)$$

$$2(1 - U_k - y) = 2\alpha_5 \quad (18)$$

$$y = z \quad (19)$$

In the calculations, Microsoft Excel Solver was used to compute the UFL values of the alkanes,  $U_{ks}$ , by solving Eq. (8) with Eqs. (13)–(19).

### 3. RESULTS AND DISCUSSION

The vessel shown in Figure 1 is first discussed in this section. Flammability-limit experiments have frequently been conducted in vessels recommended by several standards. For instance, a European standard<sup>32</sup> uses a cylindrical or spherical vessel with a volume of  $>5 \text{ dm}^3$ . Flammability limits typically vary depending on the experimental conditions, including the vessel volume. This reflects that the influences of flame quenching at the vessel wall are not negligible in the case of small vessels (i.e., heat loss), which generally increases the LFL and decreases the UFL. In this study, a vessel with a higher surface area-to-volume ratio than the standard vessel was used. However, we confirmed no significant differences in terms of the LFL and UFL of a  $\text{CH}_4$ –air mixture between the experimental values in the vessel and literature values (in this study, LFL =

4.9 vol% UFL = 15.4 vol%; in the literature, LFL = ca. 5 vol% and UFL = 15 vol%).<sup>39</sup> Hence, errors due to heat loss in the small vessel were considered relatively small.

### 3.1. LFLs and UFLs of CH<sub>4</sub>-N<sub>2</sub>O-diluent mixtures

Figure 2 shows the ternary flammability diagrams for the CH<sub>4</sub>-N<sub>2</sub>O-diluent mixtures in which the concentrations of the components are plotted on the three axes. In the figure, LFLs and UFLs are shown in black open circles and blue-green squares, respectively, and  $Y_D$  denotes the concentration of the diluent (i.e.,  $Y_{N_2}$ ,  $Y_{Ar}$ , and  $Y_{CO_2}$ ). As shown in Figure 2a, the LFL and UFL values remained almost constant and linearly decreased with an increase in the diluent N<sub>2</sub> concentration, respectively. When the  $Y_{N_2}$  value reached 65.1 vol%, no increase in explosion pressure was recorded. Thus, the MIC of the CH<sub>4</sub>-N<sub>2</sub>O-N<sub>2</sub> mixture was determined to be 65.1 vol%. The LN<sub>2</sub>OC of the CH<sub>4</sub>-N<sub>2</sub>O-N<sub>2</sub> mixture was 30.0 vol%. The LFL and UFL values at an  $Y_{N_2} = 0$  vol% were 2.5 and 40.5 vol%, respectively. The values obtained in this study are nearly consistent with the literature values<sup>40</sup>, which were determined using a 4.2-dm<sup>3</sup> spherical vessel. Hence, this also implies that the heat loss owing to the small vessel used in this study is negligible.

Figures 2b and c display the ternary flammability diagrams for the CH<sub>4</sub>-N<sub>2</sub>O-Ar and CH<sub>4</sub>-N<sub>2</sub>O-CO<sub>2</sub> mixtures, respectively. Similar to the CH<sub>4</sub>-N<sub>2</sub>O-N<sub>2</sub> mixture shown in Figure 2a, the same dependency of the LFL and UFL behaviors on the diluent concentrations was observed for the CH<sub>4</sub>-N<sub>2</sub>O-Ar and CH<sub>4</sub>-N<sub>2</sub>O-CO<sub>2</sub> mixtures: the LFL and UFL values remained unchanged and linearly decreased with increasing diluent concentration, respectively. The LN<sub>2</sub>OCs of the CH<sub>4</sub>-N<sub>2</sub>O-Ar and CH<sub>4</sub>-N<sub>2</sub>O-CO<sub>2</sub> mixtures were found to be 24.4 and 40.1 vol%, respectively. The

MIC values of the CH<sub>4</sub>-N<sub>2</sub>O-Ar and CH<sub>4</sub>-N<sub>2</sub>O-CO<sub>2</sub> mixtures were  $Y_{Ar} = 70.2$  vol% and  $Y_{CO_2} = 53.1$  vol%, respectively.

Table 1 provides the LFL, UFL, LN<sub>2</sub>OC, and MIC values of the CH<sub>4</sub>-N<sub>2</sub>O-N<sub>2</sub>, CH<sub>4</sub>-N<sub>2</sub>O-Ar, and CH<sub>4</sub>-N<sub>2</sub>O-CO<sub>2</sub> mixtures. The inerting ability can be generally ranked in the following order: CO<sub>2</sub> > H<sub>2</sub>O > N<sub>2</sub> > He > Ar.<sup>41</sup> Apart from helium, this ranking reflects the order of the heat capacity—the distinguishing property of helium is attributed to its high thermal conductivity. The MIC order in the N<sub>2</sub>O atmosphere in this study agrees well with the inerting ability of the diluents.

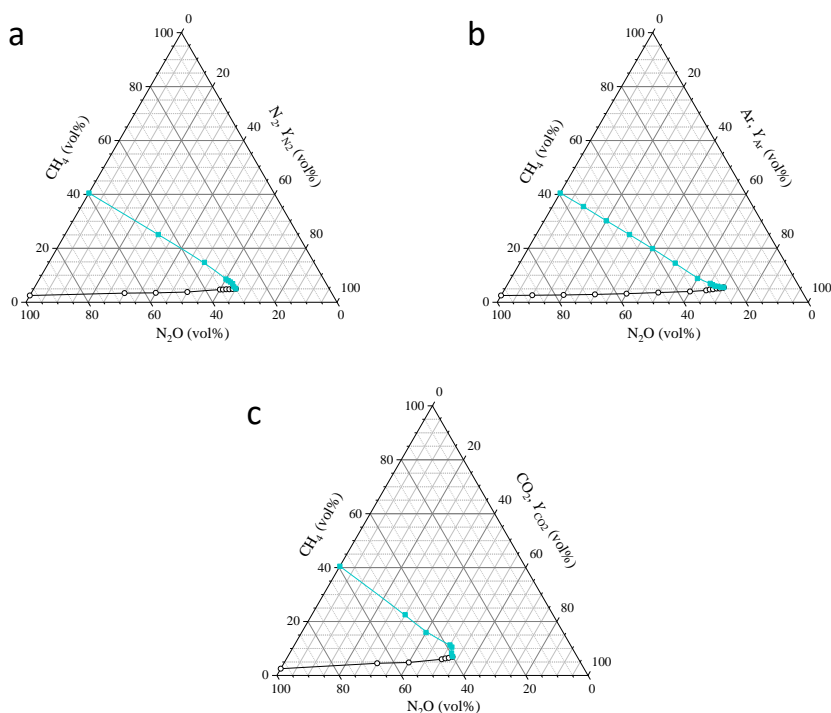


Figure 2 Ternary flammability diagrams for CH<sub>4</sub>-N<sub>2</sub>O-diluent mixtures. (a) CH<sub>4</sub>-N<sub>2</sub>O-N<sub>2</sub>, (b) CH<sub>4</sub>-N<sub>2</sub>O-Ar, and (c) CH<sub>4</sub>-N<sub>2</sub>O-CO<sub>2</sub> mixtures. The black open circles and curves and blue-green closed squares and curves represent the LFLs and UFLs of CH<sub>4</sub>-N<sub>2</sub>O-diluent mixtures, respectively.

Table 1. LFLs, UFLs, LN<sub>2</sub>OCs, and MICs of the CH<sub>4</sub>-N<sub>2</sub>O-diluent mixtures tested in this study.

Mixture	LFL (vol%)	UFL (vol%)	LN <sub>2</sub> OC (vol%)	MIC (vol%)
CH <sub>4</sub> -N <sub>2</sub> O-N <sub>2</sub>	2.5	40.5	30.0	65.1
CH <sub>4</sub> -N <sub>2</sub> O-Ar	idem	idem	24.4	70.2
CH <sub>4</sub> -N <sub>2</sub> O-CO <sub>2</sub>	idem	idem	40.1	53.1

LFL: Lower flammability limit; UFL: Upper flammability limit; LN<sub>2</sub>OC: Limit nitrous oxide concentration; and MIC: Minimum inerting concentration.

### 3.2. LFLs and UFLs of C<sub>3</sub>H<sub>8</sub>-N<sub>2</sub>O-diluent mixtures

The ternary flammability diagrams for the C<sub>3</sub>H<sub>8</sub>-N<sub>2</sub>O-diluent mixtures are shown in [Figure 3](#). The LFLs and UFLs of the mixtures are presented in black open circles and blue closed squares in the figure, respectively. Like the corresponding CH<sub>4</sub>-N<sub>2</sub>O-diluent mixtures, their LFLs remained almost unchanged with increasing  $Y_D$  values, whereas their UFLs linearly decreased with  $Y_D$  values. The MIC values of the C<sub>3</sub>H<sub>8</sub>-N<sub>2</sub>O-N<sub>2</sub>, C<sub>3</sub>H<sub>8</sub>-N<sub>2</sub>O-Ar, and C<sub>3</sub>H<sub>8</sub>-N<sub>2</sub>O-CO<sub>2</sub> mixtures were  $Y_{N_2} = 65.2$ ,  $Y_{Ar} = 69.5$ , and  $Y_{CO_2} = 58.4$  vol%, respectively. Shebeko et al.<sup>42</sup>, in their investigation of the MIC using a 56.52-dm<sup>3</sup> cylindrical explosion vessel, reported an MIC of 60.0 vol% for the C<sub>3</sub>H<sub>8</sub>-N<sub>2</sub>O-CO<sub>2</sub> mixture, which is almost consistent with the value determined in this study. The LFL and UFL of the C<sub>3</sub>H<sub>8</sub>-N<sub>2</sub>O mixture (i.e.,  $Y_D = 0$  vol%) were 1.4 and 24.0 vol%, respectively.

[Table 2](#) summarizes the LFL, UFL, LN<sub>2</sub>OC, and MIC values of the C<sub>3</sub>H<sub>8</sub>-N<sub>2</sub>O-N<sub>2</sub>, C<sub>3</sub>H<sub>8</sub>-N<sub>2</sub>O-Ar, and C<sub>3</sub>H<sub>8</sub>-N<sub>2</sub>O-CO<sub>2</sub> mixtures. Like the CH<sub>4</sub>-N<sub>2</sub>O-diluent mixtures discussed in [Section 3.1](#), the order of the MIC was well consistent with the inerting ability of the diluents (i.e., MIC: CO<sub>2</sub> > N<sub>2</sub> > Ar).

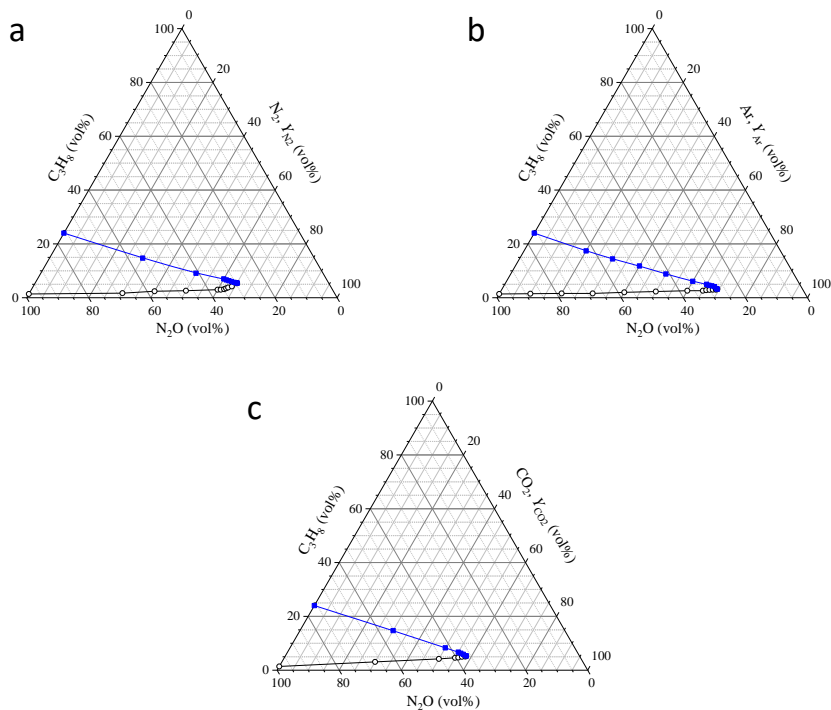


Figure 3 Ternary flammability diagrams for  $C_3H_8$ - $N_2O$ -diluent mixtures. (a)  $C_3H_8$ - $N_2O$ - $N_2$ , (b)  $C_3H_8$ - $N_2O$ -Ar, and (c)  $C_3H_8$ - $N_2O$ - $CO_2$  mixtures. The black open circles and curves and blue closed squares and curves represent the LFLs and UFLs of  $C_3H_8$ - $N_2O$ -diluent mixtures, respectively.

Table 2 LFLs, UFLs,  $LN_2OC$ s, and MICs of  $C_3H_8$ - $N_2O$ -diluent mixtures tested in this study.

Mixture	LFL (vol%)	UFL (vol%)	$LN_2OC$ (vol%)	MIC (vol%)
$C_3H_8$ - $N_2O$ - $N_2$	1.4	24.0	29.5	65.2
$C_3H_8$ - $N_2O$ -Ar	idem	idem	27.4	69.5
$C_3H_8$ - $N_2O$ - $CO_2$	idem	idem	36.5	58.4

LFL: Lower flammability limit; UFL: Upper flammability limit;  $LN_2OC$ : Limit nitrous oxide concentration; and MIC: Minimum inerting concentration.

### 3.3. Equilibrium compositions and AFTs of upper-limit CH<sub>4</sub>-N<sub>2</sub>O-diluent mixtures

As described in [Section 1.2](#), the UFLs of the n-alkane-N<sub>2</sub>O-diluent mixtures will hereinafter be addressed. The thermochemical equilibrium calculations revealed that the molar fractions of N<sub>2</sub>O for the CH<sub>4</sub>-N<sub>2</sub>O-N<sub>2</sub>, CH<sub>4</sub>-N<sub>2</sub>O-Ar, and CH<sub>4</sub>-N<sub>2</sub>O-CO<sub>2</sub> mixtures were  $<4.9 \times 10^{-7}$ ,  $<2.3 \times 10^{-7}$ , and  $<2.3 \times 10^{-7}$ , respectively, thereby providing evidence that almost all N<sub>2</sub>O decomposed during combustion into N<sub>2</sub> and O<sub>2</sub> according to [Eq. \(1\)](#). The findings are consistent with the fact that the decomposition into N<sub>2</sub> and O<sub>2</sub> occurs at  $>600$  °C,<sup>43</sup> as discussed in the section on the flame temperature immediately below.

As an example of typical calculation results, the equilibrium compositions and AFTs of the upper-limit CH<sub>4</sub>-N<sub>2</sub>O-Ar mixture as a function of  $Y_{Ar}$  are depicted in [Figure 4](#) because similar trends in the equilibrium compositions and AFTs are found for the CH<sub>4</sub>-N<sub>2</sub>O-N<sub>2</sub> and CH<sub>4</sub>-N<sub>2</sub>O-CO<sub>2</sub> mixtures. In this figure, only chemical species with molar fractions of  $>10^{-4}$  are plotted. As reported by Palucis et al.<sup>44</sup>, a typical AFT value of lower alkanes in pure O<sub>2</sub> is around 1200 K. In contrast, the AFTs of the tested CH<sub>4</sub>-N<sub>2</sub>O-diluent mixtures were  $>2000$  K, which is well consistent with an earlier study's finding that fuel-N<sub>2</sub>O mixtures exhibited higher AFTs compared with the corresponding fuel-O<sub>2</sub> mixture.<sup>16</sup> The calculations also indicate a nonlinear relationship between AFT and  $Y_{Ar}$ .

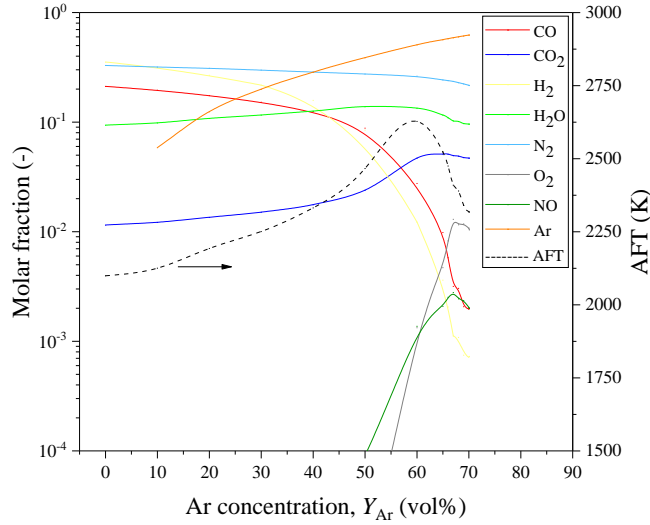


Figure 4 Equilibrium compositions (the solid curves) and AFT (the broken curve) for upper-limit  $\text{CH}_4\text{-N}_2\text{O-Ar}$  mixture as a function of  $Y_{\text{Ar}}$ . In this figure, only chemical species with molar fractions of  $>10^{-4}$  are depicted.

As shown in Figure 4, the thermochemical equilibrium calculations proved that the molar fractions of NO and  $\text{O}_2$ , which are generated from the decomposition of  $\text{N}_2\text{O}$  (Eq. (1)), were  $<10^{-2}$ , whereas those of CO,  $\text{CO}_2$ ,  $\text{H}_2$ ,  $\text{H}_2\text{O}$ ,  $\text{N}_2$ , and Ar were  $>10^{-2}$ . The findings allowed us to conclude that the major species of the upper-limit  $\text{CH}_4\text{-N}_2\text{O-Ar}$  mixtures are CO,  $\text{CO}_2$ ,  $\text{H}_2$ ,  $\text{H}_2\text{O}$ ,  $\text{N}_2$ , and Ar (i.e., the diluent). Hence, when mathematically estimating the UFLs of the  $\text{CH}_4\text{-N}_2\text{O-Ar}$  mixture from Eq. (8) with Eqs. (13)–(19), the following six species were used: CO,  $\text{CO}_2$ ,  $\text{H}_2$ ,  $\text{H}_2\text{O}$ ,  $\text{N}_2$ , and Ar.

The thermochemical equilibrium calculations also confirmed similar trends for the  $\text{CH}_4\text{-N}_2\text{O-N}_2$  and  $\text{CH}_4\text{-N}_2\text{O-CO}_2$  mixtures. Thus, when calculating the UFLs of the  $\text{CH}_4\text{-N}_2\text{O-N}_2$  and  $\text{CH}_4\text{-N}_2\text{O-CO}_2$  mixtures using Eqs. (8) and (13)–(19), the following five chemical species were used: CO,  $\text{CO}_2$ ,  $\text{H}_2$ ,  $\text{H}_2\text{O}$ , and  $\text{N}_2$ . Note that five chemical species were used in the calculations instead

of six because the diluent and chemical species (i.e., CO<sub>2</sub> and N<sub>2</sub>) generated during combustion are the same.

### 3.4. Equilibrium compositions and AFTs of upper-limit C<sub>3</sub>H<sub>8</sub>–N<sub>2</sub>O–diluent mixtures

The thermochemical equilibrium calculations verified that the molar fractions of N<sub>2</sub>O for the C<sub>3</sub>H<sub>8</sub>–N<sub>2</sub>O–N<sub>2</sub>, C<sub>3</sub>H<sub>8</sub>–N<sub>2</sub>O–Ar, and C<sub>3</sub>H<sub>8</sub>–N<sub>2</sub>O–CO<sub>2</sub> mixtures were  $<6.6 \times 10^{-11}$ ,  $<4.1 \times 10^{-8}$ , and  $<4.9 \times 10^{-10}$ , respectively. According to Eq. (1), a small amount of N<sub>2</sub>O remained after combustion, implying that it was almost completely decomposed.

As an example, Figure 5 depicts the equilibrium compositions and AFTs of the upper-limit C<sub>3</sub>H<sub>8</sub>–N<sub>2</sub>O–Ar mixtures versus  $Y_{Ar}$ . In this figure, only chemical species with molar fractions of  $>10^{-4}$  are shown. Like the upper-limit CH<sub>4</sub>–N<sub>2</sub>O–Ar mixture, the AFT varied nonlinearly within a range of 1903 K–2488 K, which is higher than that of the corresponding C<sub>3</sub>H<sub>8</sub>–O<sub>2</sub> mixture.<sup>16</sup>

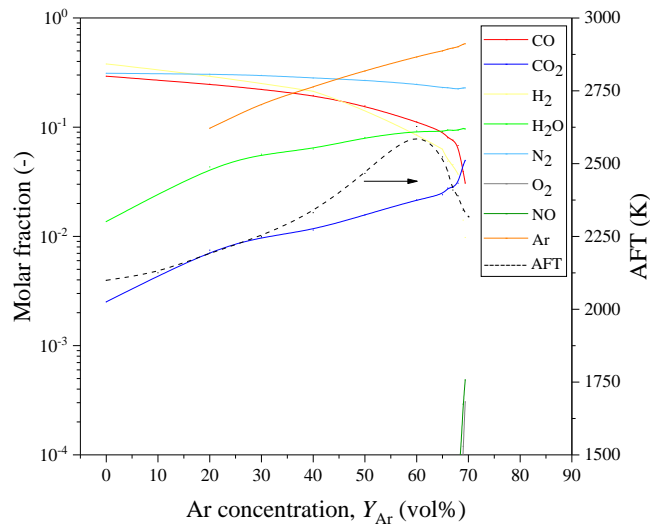


Figure 5 Equilibrium compositions (the solid curves) and AFTs (the broken curve) of upper-limit  $C_3H_8-N_2O-Ar$  mixture as a function of  $Y_{Ar}$ . In this figure, only chemical species with molar fractions of  $>10^{-4}$  are shown.

The thermochemical equilibrium calculations provide undisputed evidence that the major chemical species of the upper-limit  $C_3H_8-N_2O-Ar$  mixture during combustion are  $CO$ ,  $CO_2$ ,  $H_2$ ,  $H_2O$ ,  $N_2$ , and  $Ar$ . Furthermore, similar trends for the  $C_3H_8-N_2O-N_2$  and  $C_3H_8-N_2O-CO_2$  mixtures were observed, thereby suggesting the use of the following five and six chemical species in the calculations using Eqs. (8) and (13)–(19) to calculate the UFLs of the  $C_3H_8-N_2O$ -diluent mixture:  $CO$ ,  $CO_2$ ,  $H_2$ ,  $H_2O$ ,  $N_2$ , and the diluent.

### 3.5. Calculations of UFLs of $CH_4-N_2O$ -diluent and $C_3H_8-N_2O$ -diluent mixtures

Figure 6 shows the experimental and computed UFLs of the  $CH_4-N_2O$ -diluent mixture as a function of  $Y_D$  using Eqs. (8) and Eqs. (13)–(19). Note that the experimental data (i.e., UFLs) are rewritten, which are the same as the data plotted in Figure 2. In Figure 6, the solid curves were computed. As shown in Figures 6a and 6b, the comparisons of the experimental UFLs with the calculated UFLs indicate no significant differences between the experimental and computed data. In contrast, for the upper-limit  $CH_4-N_2O-CO_2$  mixture, some differences in the UFL between the experimental and calculated data were observed. However, for the upper-limit  $CH_4-N_2O-CO_2$  mixture, the mathematical calculation produced the safe-side output, indicating that the calculations are not meaningless.

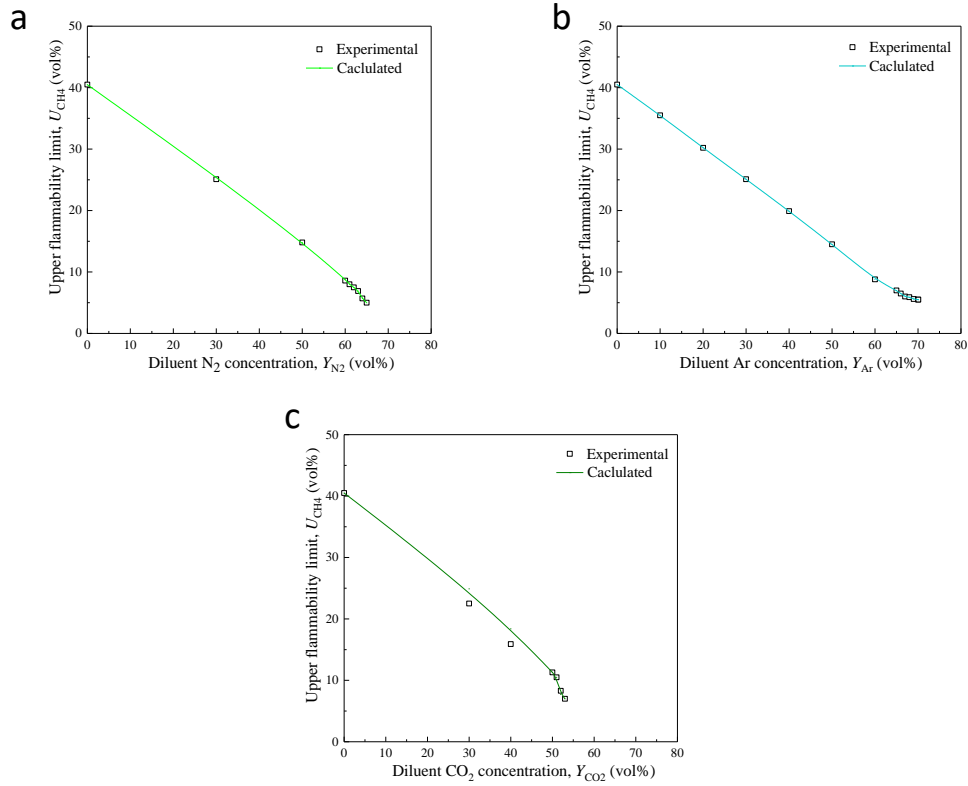


Figure 6 UFLs of CH<sub>4</sub>-N<sub>2</sub>O-diluent mixture as a function of  $Y_D$ . (a) CH<sub>4</sub>-N<sub>2</sub>O-N<sub>2</sub>, (b) CH<sub>4</sub>-N<sub>2</sub>O-Ar, and (c) CH<sub>4</sub>-N<sub>2</sub>O-CO<sub>2</sub>. The squares represent the experimental data obtained in this study, which is same as Figure 2. The colored solid curves are computed using Eq. (8) and Eqs. (13)–(19).

Table 3 lists the MAPE values calculated using Eq. (3) for the upper-limit CH<sub>4</sub>-N<sub>2</sub>O-N<sub>2</sub>, CH<sub>4</sub>-N<sub>2</sub>O-Ar, and CH<sub>4</sub>-N<sub>2</sub>O-CO<sub>2</sub> mixtures. Generally, “forecasts are potentially very good” when MAPE is 10% or less.<sup>45</sup> The findings enable us to conclude that the experimental UFLs were successfully computed using Eqs. (8) and (13)–(19).

However, as described above, the CH<sub>4</sub>-N<sub>2</sub>O-CO<sub>2</sub> mixture had a relatively higher MAPE value than the CH<sub>4</sub>-N<sub>2</sub>O-N<sub>2</sub> and CH<sub>4</sub>-N<sub>2</sub>O-Ar mixtures. In the calculations, soot generated from the

incomplete combustion of the upper-limit mixtures, attributed to the insufficient concentration of the oxidizer, is not considered. In addition, Fishburne et al. provided evidence of the thermal dissociation of  $\text{CO}_2$  to  $\text{CO}$  and  $\text{C}$ .<sup>46</sup> The differences in the UFL between the experimental and calculated values perhaps arise from these factors.

Table 3 MAPEs for upper-limit  $\text{CH}_4\text{-N}_2\text{O}$ -diluent mixtures.

Mixture	MAPE (%)
Upper-limit $\text{CH}_4\text{-N}_2\text{O-N}_2$	0.35
Upper-limit $\text{CH}_4\text{-N}_2\text{O-Ar}$	0.03
Upper-limit $\text{CH}_4\text{-N}_2\text{O-CO}_2$	2.82

MAPE: Mean absolute percentage error.

Figure 7 displays the experimental and calculated UFLs of the  $\text{C}_3\text{H}_8\text{-N}_2\text{O}$ -diluent mixtures as a function of  $Y_D$  using Eqs. (8) and (13)–(19). Once more, the UFLs are replotted in the figure. Like the  $\text{CH}_4\text{-N}_2\text{O}$ -diluent mixtures, there are no significant differences between the experimental and calculated UFLs of the  $\text{C}_3\text{H}_8\text{-N}_2\text{O-N}_2$  and  $\text{C}_3\text{H}_8\text{-N}_2\text{O-Ar}$  mixtures. Conversely, non-negligible differences between the experimental and estimated UFLs of the  $\text{C}_3\text{H}_8\text{-N}_2\text{O-CO}_2$  mixture were found, which followed the same trend as the  $\text{CH}_4\text{-N}_2\text{O-CO}_2$  mixture.

The MAPE values for the upper-limit  $\text{C}_3\text{H}_8\text{-N}_2\text{O-N}_2$ ,  $\text{C}_3\text{H}_8\text{-N}_2\text{O-Ar}$ , and  $\text{C}_3\text{H}_8\text{-N}_2\text{O-CO}_2$  mixtures were calculated to be 0.41%, 0.41%, and 4.11%, respectively (Table 4). The higher error for the  $\text{C}_3\text{H}_8\text{-N}_2\text{O-CO}_2$  mixture is also due to the same reason as that for the  $\text{CH}_4\text{-N}_2\text{O-CO}_2$  mixture.

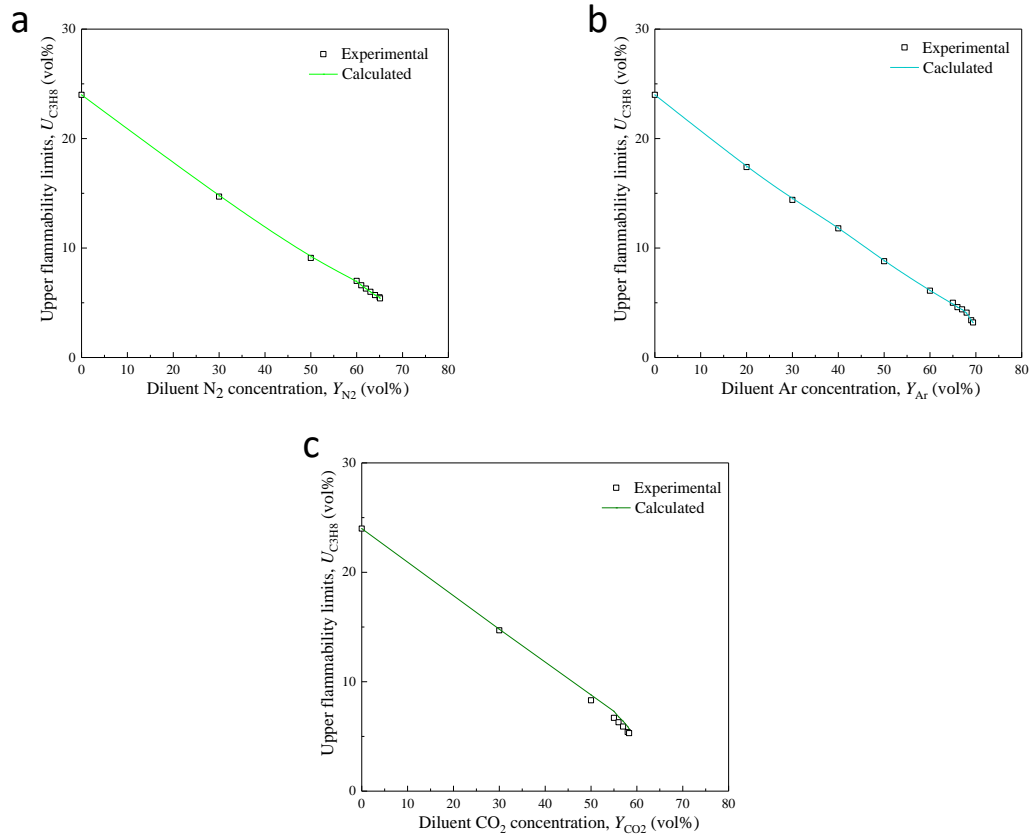


Figure 7 UFLs of  $C_3H_8-N_2O$ -diluent mixture as a function of  $Y_D$ . (a)  $C_3H_8-N_2O-N_2$ , (b)  $C_3H_8-N_2O-Ar$ , and (c)  $C_3H_8-N_2O-CO_2$ . The squares represent the experimental data obtained in this study, which is same as in Figure 3. The colored solid curves are computed from Eq. (8) and Eqs. (13)–(19).

Table 4 MAPEs for upper-limit  $C_3H_8-N_2O$ -diluent mixtures.

Mixture	MAPE (%)
Upper-limit $C_3H_8-N_2O-N_2$	0.41
Upper-limit $C_3H_8-N_2O-Ar$	0.41
Upper-limit $C_3H_8-N_2O-CO_2$	4.11

MAPE: Mean absolute percentage error.

In summary, this research has demonstrated the use of appropriate five and six chemical species (i.e., CO, CO<sub>2</sub>, H<sub>2</sub>O, H<sub>2</sub>, N<sub>2</sub>, and Ar) and Eqs. (8) and (13)–(19) to mathematically estimate the UFLs of the CH<sub>4</sub>–N<sub>2</sub>O–diluent and C<sub>3</sub>H<sub>8</sub>–N<sub>2</sub>O–diluent mixtures with MAPEs of  $\leq 2.82$  and  $\leq 4.11\%$ , respectively. So far, no papers have been published on the estimation of the UFLs of the fuel–N<sub>2</sub>O mixtures diluted with inert gases. As mentioned in Section 1, N<sub>2</sub>O is widely used as an oxidizer in laboratories and industries. Hence, this study provides novel and valuable contributions to related research.

The key findings of this study will provide insight into understanding the flammability limits of n-alkane–N<sub>2</sub>O mixtures. An N<sub>2</sub>O release accident in a chemical plant that handles large amounts of N<sub>2</sub>O could have a considerable impact on the environment due to the global warming and ozone-depleting potentials of N<sub>2</sub>O, resulting in N<sub>2</sub>O not being used in large-scale chemical plants in the future. While the flammability limits of gas mixtures containing air and O<sub>2</sub> as oxidizers have been well studied, those of gas mixtures containing other oxidizing gases have not been thoroughly investigated in the literature. Systematically studying the effects of oxidizers on the flammability limits of gas mixtures is crucial from an academic viewpoint, and it has potential to make a considerable contribution to assessing and reducing fire/explosion risks in laboratories and industries where various oxidizers are handled and stored.

#### 4. CONCLUSIONS

In this study, the LFLs, UFLs, LN<sub>2</sub>OCs, and MICs of the CH<sub>4</sub>–N<sub>2</sub>O–diluent and C<sub>3</sub>H<sub>8</sub>–N<sub>2</sub>O–diluent mixtures (diluent: N<sub>2</sub>, Ar, and CO<sub>2</sub>) were experimentally investigated. Furthermore, the

UFLs of the CH<sub>4</sub>-N<sub>2</sub>O-diluent and C<sub>3</sub>H<sub>8</sub>-N<sub>2</sub>O-diluent mixtures were computationally estimated using Eqs. (8) and (13)–(19). The major findings can be outlined as follows:

- i. The LFLs of the CH<sub>4</sub>-N<sub>2</sub>O-diluent and C<sub>3</sub>H<sub>8</sub>-N<sub>2</sub>O-diluent mixtures were experimentally determined to be 2.5 and 1.4 vol%, respectively, and were little dependent on  $Y_D$ . The UFLs of the CH<sub>4</sub>-N<sub>2</sub>O-diluent and C<sub>3</sub>H<sub>8</sub>-N<sub>2</sub>O-diluent mixtures were 40.5 and 24.0 vol%, respectively, and linearly decreased with increasing  $Y_D$ .
- ii. The LN<sub>2</sub>OCs of the CH<sub>4</sub>-N<sub>2</sub>O-N<sub>2</sub>, CH<sub>4</sub>-N<sub>2</sub>O-Ar, CH<sub>4</sub>-N<sub>2</sub>O-CO<sub>2</sub>, C<sub>3</sub>H<sub>8</sub>-N<sub>2</sub>O-N<sub>2</sub>, C<sub>3</sub>H<sub>8</sub>-N<sub>2</sub>O-Ar, and C<sub>3</sub>H<sub>8</sub>-N<sub>2</sub>O-CO<sub>2</sub> mixtures were 30.0, 24.4, 40.1, 29.6, 27.4, and 26.5 vol%, respectively. The MICs of the CH<sub>4</sub>-N<sub>2</sub>O-N<sub>2</sub>, CH<sub>4</sub>-N<sub>2</sub>O-Ar, CH<sub>4</sub>-N<sub>2</sub>O-CO<sub>2</sub>, C<sub>3</sub>H<sub>8</sub>-N<sub>2</sub>O-N<sub>2</sub>, C<sub>3</sub>H<sub>8</sub>-N<sub>2</sub>O-Ar, and C<sub>3</sub>H<sub>8</sub>-N<sub>2</sub>O-CO<sub>2</sub> mixtures were 65.1, 70.2, 53.1, 65.2, 69.5, and 58.4 vol%, respectively, indicating that the order of the MICs in N<sub>2</sub>O atmosphere was well consistent with the inerting ability of the diluents: CO<sub>2</sub> > N<sub>2</sub> > Ar.
- iii. By using six (CO, CO<sub>2</sub>, H<sub>2</sub>, H<sub>2</sub>O, N<sub>2</sub>, and Ar) or five (CO, CO<sub>2</sub>, H<sub>2</sub>, H<sub>2</sub>O, and N<sub>2</sub>) chemical species and Eqs. (8) and (13)–(19), we mathematically estimated the UFLs of the CH<sub>4</sub>-N<sub>2</sub>O-diluent and C<sub>3</sub>H<sub>8</sub>-N<sub>2</sub>O-diluent mixtures with MAPEs of ≤2.82% and ≤4.11%, respectively.

In conclusion, the semi-empirical model presented in this study would provide proof of concept that the UFLs of n-alkane-N<sub>2</sub>O-diluent mixtures can be estimated with small deviations. This valuable finding could significantly contribute to reducing accident-induced losses in industries and laboratories that handle and store N<sub>2</sub>O.

## AUTHOR INFORMATION

### Corresponding Author

Yusuke Koshiha – Department of Materials Science and Chemical Engineering, Faculty of Engineering, Yokohama National University, 79-5 Tokiwadai, Hodogaya-ku, Yokohama 240-8501, Japan; orcid.org/0000-0003-3448-1458; Email: koshiha-yusuke-xm@ynu.ac.jp

### **Authors**

Yusuke Koshiha – Department of Materials Science and Chemical Engineering, Faculty of Engineering, Yokohama National University, 79-5 Tokiwadai, Hodogaya-ku, Yokohama 240-8501, Japan.

Shiho Asano – Graduate School of Environmental and Information Sciences, Yokohama National University, 79-7 Tokiwadai, Hodogaya-ku, Yokohama 240-8501, Japan

### **Author contributions**

*Yusuke Koshiha*: Conceptualization, methodology, investigation, software, data curation, project administration, and writing. *Shiho Asano*: Methodology, investigation, software, and data curation.

### **Notes**

The authors declare that they have no known competing financial interests or personal relationships that could have appeared to influence the work reported in this paper.

### **ABBREVIATIONS**

$a_{1-7}$  Constants in Eqs. (4)–(6)

AFT Adiabatic flame temperature (K)

$C_{st}$  Stoichiometric concentration (vol%)

$c_p$  Heat capacity at constant pressure ( $J K^{-1} mol^{-1}$ )

- $D$  Diluent (i.e.,  $N_2$ , Ar, and  $CO_2$ )
- $H$  Enthalpy ( $J\ mol^{-1}$ )
- $\Delta H_c$  Enthalpy of combustion in Eq. (8) ( $J\ mol^{-1}$ )
- $\Delta H_{c,k}$  Enthalpy of the combustion reactions for chemical species  $k$  ( $J\ mol^{-1}$ )
- $H_k^{ad}$  Enthalpy of chemical species  $k$  at the AFT ( $J\ mol^{-1}$ )
- $H_k^0$  Enthalpy of chemical species  $k$  at  $25\ ^\circ C$  ( $J\ mol^{-1}$ )
- $k$  Constant in Eq. (2) or chemical species
- LFL Lower flammability limit (vol%)
- $LN_2OC$  Limit nitrous oxide concentration (vol%)
- $m$  Number of hydrogen in the n-alkane:  $m = 2n + 2$  (Eq. (9))
- MAPE Mean absolute percentage error (%)
- MIC Minimum inerting concentration (vol%)
- $n$  Number of carbon in the n-alkane (Eq. (9)) or number of the data points in Eq. (3)
- $P$  Pressure (MPa)
- $R$  Gas constant ( $8.31\ J\ K^{-1}\ mol^{-1}$ )
- $S$  Entropy ( $J\ K^{-1}\ mol^{-1}$ )
- $T$  Temperature (K)

- UFL Upper flammability limit (vol%)
- $U_k$  UFL of n-alkane  $k$  (vol%)
- $V_e$  Estimated value in Eq. (3)
- $V_a$  Actual value in Eq. (3)
- $X_k$  Molar concentration of chemical species  $k$  (mol m<sup>-3</sup>)
- $Y_D$  Concentration of the diluent (vol%)
- $y$  Molar fraction of the diluent in Eqs. (8), (14), and (17)–(19) (dimensionless)
- $z$  Stoichiometric coefficient in Eq. (8)
- $\alpha_1$ – $\alpha_4$  Stoichiometric coefficients in Eq. (8) and Eqs. (13)–(18)

## REFERENCES

- (1) Cutchin, M. P.; Martin, K. R.; Owen, S. V.; Goodwin, J. S. Concern about petrochemical health risk before and after a refinery explosion. *Risk Anal.* **2008**, 28, 589–601. <https://doi.org/10.1111/j.1539-6924.2008.01050.x>
- (2) Jira, R. J. Acetaldehyde from ethylene—A retrospective on the discovery of the Wacker process. *Angew. Chem. Int Ed Engl* **2009**, 48, 9034–9037. <https://doi.org/10.1002/anie.200903992>
- (3) Sano, K.; Koshiba, Y.; Ohtani, H. Risk assessment and risk reduction of an acrylonitrile production plant. *J. Loss Prev. Process Ind.* **2020**, 63, 104015. <https://doi.org/10.1016/j.jlp.2019.104015>

- (4) Newman, S. G.; Lee, K.; Cai, J.; Yang, L.; Green, W. H.; Jensen, K. F. Continuous thermal oxidation of alkenes with nitrous oxide in a packed bed reactor. *Ind. Eng. Chem. Res.* **2015**, *54*, 4166–4173. <https://doi.org/10.1021/ie504129e>
- (5) Montzka, S. A.; Dlugokencky, E. J.; Butler, J. H. Non-CO<sub>2</sub> greenhouse gases and climate change. *Nature* **2011**, *476*, 43–50. <https://doi.org/10.1038/nature10322>
- (6) Razus, D. Nitrous oxide: Oxidizer and promoter of hydrogen and hydrocarbon combustion. *Ind. Eng. Chem. Res.* **2022**, *61*, 11329–11346. <https://doi.org/10.1021/acs.iecr.2c01774>
- (7) Parfenov, M. V.; Ivanov, D. P.; Kharitonov, A. S.; Dubkov, K. A. Gas-phase selective oxidation of butenes in the C<sub>4</sub> fraction by nitrous oxide. *Ind. Eng. Chem. Res.* **2022**, *61*, 8607–8615. <https://doi.org/10.1021/acs.iecr.2c00694>
- (8) Le Vaillant F.; Mateos Calbet, A.; González-Pelayo, S.; Reijerse, E. J.; Ni, S.; Busch, J.; Cornella, J. Catalytic synthesis of phenols with nitrous oxide. *Nature* **2022**, *604*, 677–683. <https://doi.org/10.1038/s41586-022-04516-4>
- (9) Cornell, R. E.; Barbet, M. C.; Burke, M. P. Toward a more comprehensive understanding of the kinetics of a common biomass-derived impurity: NH<sub>3</sub> oxidation by N<sub>2</sub>O in a jet-stirred reactor. *Energy Fuels* **2021**, *35*, 13338–13348. <https://doi.org/10.1021/acs.energyfuels.1c01544>
- (10) U.S. Chemical Safety and Hazard Investigation Board. Nitrous oxide explosion. Investigation report (Report number: #2016-04-I-FL; Issue date: Feb. 2017).
- (11) Sonnemans, P. J. M.; Körvers, P. M. W. Accidents in the chemical industry: Are they foreseeable? *J. Loss Prev. Process Ind.* **2006**, *19*, 1–12. <https://doi.org/10.1016/j.jlp.2005.03.008>

- (12) Drysdale, D. An introduction to fire dynamics, third ed. Wiley, West Sussex, pp. 83–97, **2011**.
- (13) Crowl, D. A.; Louvar, J. F. Chemical process safety: Fundamentals with applications, third ed. Pearson Education, Inc., Boston. **2011**.
- (14) Abdelkhalik, A.; Askar, E.; Markus, D.; Stolz, T.; Brandes, E.; Zakel, S.; Explosion regions of 1,3-dioxolane/nitrous oxide and 1,3-dioxolane/air with different inert gases—Experimental data and numerical modelling. *J. Loss Prev. Process Ind.* **2021**, 71, 104496. <https://doi.org/10.1016/j.jlp.2021.104496>
- (15) Koshiha, Y.; Takigawa, T.; Matsuoka, Y.; Ohtani, H. Explosion characteristics of flammable organic vapors in nitrous oxide atmosphere. *J. Hazard. Mater.* **2010**, 183, 746–753. <https://doi.org/10.1016/j.jhazmat.2010.07.089>
- (16) Koshiha, Y.; Nishida, T.; Morita, N.; Ohtani, H. Explosion behavior of n-alkane/nitrous oxide mixtures. *Process Saf. Environ. Prot.* **2015**, 98, 11–15. <https://doi.org/10.1016/j.psep.2015.06.005>
- (17) Vandebroek, L.; Van den Schoor, F.; Verplaetsen, F.; Berghmans, J.; Winter, H.; van't Oost, E. Flammability limits and explosion characteristics of toluene–nitrous oxide mixtures. *J. Hazard. Mater.* **2005**, 120, 57–65. <https://doi.org/10.1016/j.jhazmat.2005.01.016>
- (18) Hu, X.; Xie, Q.; Yu, Q.; Liu, H.; Yan, F. Effects of carbon dioxide on the lower flammability limit of propane in O<sub>2</sub>/CO<sub>2</sub> atmosphere. *Energy Fuels* **2020**, 34, 4993–4998. <https://doi.org/10.1021/acs.energyfuels.0c00601>
- (19) Qin, S. -H.; Sun, X. -X.; Lin, W. -C.; Shu, C. -M.; You, F.; Ho, S. -C. Experimental and computational approaches for CH<sub>4</sub> and C<sub>2</sub>H<sub>4</sub> flammability zones. *Energy Fuels* **2017**, 31, 9950–9956. <https://doi.org/10.1021/acs.energyfuels.7b00457>

- (20) Jones, G. W. Inflammation limits and their practical application in hazardous industrial operations. *Chem. Rev.* **1938**, 22, 1–26. <https://doi.org/10.1021/cr60071a001>
- (21) Kondo, S.; Takizawa, K.; Takahashi, A.; Tokuhashi, K. Extended Le Chatelier's formula and nitrogen dilution effect on the flammability limits. *Fire Saf. J.* **2006**, 41, 406–417. <https://doi.org/10.1016/j.firesaf.2006.03.002>
- (22) Lazzús, J. A. Neural network/particle swarm method to predict flammability limits in air of organic compounds. *Thermchim. Acta* **2011**, 512, 150–156. <https://doi.org/10.1016/j.tca.2010.09.018>
- (23) Kondo, S.; Takizawa, K.; Takahashi, A.; Tokuhashi, K. Measurement and numerical analysis of flammability limits of halogenated hydrocarbons. *J. Hazard. Mater.* **2004**, 109, 13–21. <https://doi.org/10.1016/j.jhazmat.2004.03.007>
- (24) Albahri, T. A. Flammability characteristics of pure hydrocarbons. *Chem. Eng. Sci.* **2003**, 58, 3629–3641. [https://doi.org/10.1016/S0009-2509\(03\)00251-3](https://doi.org/10.1016/S0009-2509(03)00251-3)
- (25) Gharagheizi, F. Chemical structure-based model for estimation of the upper flammability limit of pure compounds. *Energy Fuels* **2010**, 24, 3867–3871. <https://doi.org/10.1021/ef100207x>
- (26) Pan, Y.; Jiang, J.; Wang, R.; Cao, H.; Cui, Y. Prediction of the upper flammability limits of organic compounds from molecular structures. *Ind. Eng. Chem. Res.* **2009**, 48, 5064–5069. <https://doi.org/10.1021/ie900193r>
- (27) Liaw, H. -J.; Chen, C. -C.; Chang, C. -H.; Lin, N. -K.; Shu, C. -M. Model to estimate the flammability limits of fuel–air–diluent mixtures tested in a constant pressure vessel. *Ind. Eng. Chem. Res.* **2012**, 51, 2747–2761. <https://doi.org/10.1021/ie2011824>

- (28) Mitu, M.; Brandes, E.; Zakel, S.; Hirsch, W. Explosion regions and limiting oxygen concentrations of methyl propionate, methyl acetate, dimethyl carbonate with air and inert gas mixtures. *J. Loss Prev. Process Ind.* **2021**, *69*, 104384. <https://doi.org/10.1016/j.jlp.2020.104384>
- (29) Wu, M.; Shu, G.; Chen, R.; Tian, H.; Wang, X.; Wang, Y. A new model based on adiabatic flame temperature for evacuation of the upper flammable limit of alkane–air–CO<sub>2</sub> mixtures. *J. Hazard. Mater.* **2018**, *344*, 450–457. <https://doi.org/10.1016/j.jhazmat.2017.10.030>
- (30) Koshiba, Y.; Hasegawa, T.; Ohtani, H. Numerical and experimental study of the explosion pressures and flammability limits of lower alkenes in nitrous oxide atmosphere. *Process Saf. Environ. Prot.* **2018**, *118*, 59–67. <https://doi.org/10.1016/j.psep.2018.06.024>
- (31) Koshiba, Y.; Hasegawa, T.; Kim, B.; Ohtani, H. Flammability limits, explosion pressures, and applicability of Le Chatelier’s rule to binary alkane–nitrous oxide mixtures. *J. Loss Prev. Process Ind.* **2017**, *45*, 1–8. <http://doi.org/10.1016/j.jlp.2016.11.007>
- (32) EN 1839. Determination of the explosion limits and the limiting oxygen concentration (LOC) for flammable gases and vapours, **2017**
- (33) Kee, R. J.; Rupley, F. M.; Miller, J. A.; Coltrin, M. E.; Grcar, J. F.; Meeks, E.; Mof-fat, H. K.; Lutz, A. E.; Dixon-Lewis, G.; Smooke, M. D.; Warnatz, J.; Evans, G. H.; Larson, R. S.; Mitchell, R. E.; Petzold, L. R.; Reynolds, W. C.; Caracotsios, M.; Stewart, W. E.; Glarborg, P.; Wang, C.; McLellan, C. L.; Adigun, O.; Houf, W. G.; Chou, C. P.; Miller, S. F.; Ho, P.; Young, P. D.; Young, D. J.; Hodgson, D. W.; Petrova, M. V.; Pudukkham, K. V. CHEMKIN Release 4.1.1, Reaction Design, San Diego, CA, **2007**.
- (34) NASA Glenn Research Center. Chemical equilibrium with applications. <https://cearun.grc.nasa.gov/ThermoBuild/> (accessed 2023-03-01).

- (35) Shu, G.; Long, B.; Tian, H.; Wei, H.; Liang, X. Flame temperature theory-based model for evaluation of the flammable zones of hydrocarbon–air–CO<sub>2</sub> mixtures. *J. Hazard. Mater.* **2015**, *294*, 137–144. <https://doi.org/10.1016/j.jhazmat.2015.03.064>
- (36) Mitu, M.; Giurcan, V.; Movileanu, C.; Razus, D.; Oancea, D. Propagation of CH<sub>4</sub>–N<sub>2</sub>O–N<sub>2</sub> flames in a closed spherical vessel. *Processes* **2021**, *9*, 851. <https://doi.org/10.3390/pr9050851>
- (37) Hurley, M. J.; Gottuk, D.; Hall, J. R.; Harada, K.; Kuligowski, E.; Puchovsky, M.; Torero, J.; Watts, Jr., J.M.; Wieczorek, C. *SFPE handbook of fire protection engineering*, fifth ed. Springer. New York, pp. 325–349, **2016**. <https://doi.org/10.1007/978-1-4939-2565-0>
- (38) Drysdale, D. *An introduction to fire dynamics*, third ed. Wiley, West Sussex, pp. 1–347, **2011**.
- (39) Kundu, S.; Zanganeh, J.; Moghtaderi, B. A review on understanding explosions from methane–air mixture. *J. Loss Prev. Process Ind.* **2016**, *40*, 507–523. <https://doi.org/10.1016/j.jlp.2016.02.004>
- (40) Shebeko, A. Y.; Shebeko, Y. N.; Zuban', A. V.; Navtsenya, V. Y.; Azatyan, V. V. Influence on fluorocarbons flammability limits in the mixtures of H<sub>2</sub>–N<sub>2</sub>O and CH<sub>4</sub>–N<sub>2</sub>O. *Russ. J. Phys. Chem. B* **2014**, *8*, 65–70. <https://doi.org/10.1134/S1990793114010072>
- (41) Hurley, M. J.; Gottuk, D.; Hall, J. R.; Harada, K.; Kuligowski, E.; Puchovsky, M.; Torero, J.; Watts, Jr., J.M.; Wieczorek, C. *SFPE handbook of fire protection engineering*, fifth ed. Springer. New York, pp. 529–553, **2016**. <https://doi.org/10.1007/978-1-4939-2565-0>
- (42) Shebeko, Y. N.; Korol'chenko, A. Y.; Il'in, A. B.; Malkin, V.L. Concentration limits for flame propagation in fuel–diluent–nitrous oxide mixtures. *Combust. Explos. Shock Waves* **1988**, *24*, 306–309. <https://doi.org/10.1007/BF00750612>

- (43) Trogler, W. C. Physical properties and mechanisms of formation of nitrous oxide. *Coord. Chem. Rev.* **1999**, 187, 303–327. [https://doi.org/10.1016/S0010-8545\(98\)00254-9](https://doi.org/10.1016/S0010-8545(98)00254-9)
- (44) Palucis, M.; Van Brunt, G. V.; Ervin, E.; Chastain, W.; Kline, R.; Lodal, P. Prediction of flammability speciation for the lower alkanes, carboxylic acids, and esters. *Process Saf. Prog.* **2006**, 26, 4–9. <https://doi.org/10.1002/prs.10148>
- (45) Lewis, C. Demand forecasting and inventory control: A computer aided learning approach. Routledge, **2012**. <https://doi.org/10.4324/9781856179898>
- (46) Fishburne, E. S.; Bilwakesh, K. R.; Edse, R. Gaseous reaction rates at high temperature. I. The dissociation of carbon dioxide. *J. Chem. Phys.* **1966**, 45, 160–166. <https://doi.org/10.1063/1.1727301>